Study of Local Structure in Selected Organic–Inorganic Perovskites in the $Pm\bar{3}m$ Phase

Richard J. Worhatch,[†] HyunJeong Kim,[†] Ian P. Swainson,*[,‡] André L. Yonkeu,[‡] and Simon J. L. Billinge[†]

Department of Physics and Astronomy, Michigan State University, Biomedical Physical Sciences, East Lansing, Michigan 488242320, and Canadian Neutron Beam Centre, NRC, Chalk River Laboratories, Chalk River, Ontario K0J 1J0, Canada

Received September 18, 2007. Revised Manuscript Received December 11, 2007

The local structures of the inorganic component of selected organic–inorganic perovskites (OIPs) are studied by analyzing the X-ray pair distribution function. Whereas the long-range structure of each perovskite is the untilted $Pm\bar{3}m$ phase, all the OIPs showed significant internal distortion of the octahedra. Varying the halide has a significant impact on the lattice constant. There is evidence of local lone-pair distortions for certain compositions. The most complex case of disorder appears to be that of $CH_3NH_3SnBr_3$.

Introduction

Several organic–inorganic materials crystallize in the perovskite structure. Perovskites are a three-dimensionally bonded network structure of corner-linked octahedra.[1] Perovskites have the general formula ABX_3, where A is usually a large cation, often an alkali, and B is a metal that is octahedrally coordinated by an anion X. The common organic–inorganic perovskites (OIPs) are based around B = Ge^{2+}, Sn^{2+}, Pb^{2+}, and X is usually a halide. True perovskite structures can only contain small amines such as methylammonium, formamidinium, and tetramethylammonium:[1,2] larger cations cannot be contained in a framework and crystallize in layered structures.[2,3] Formamidinium (FA), a diamine, may be placed in a SnI_3 perovskite, in which it possesses continuous solid solution with MA.[4] It seemed likely to us that this solid solution would also exist in a $PbBr_3$-based framework, and we found this to be so. Therefore, we created an intermediate composition.

In addition to tilt transitions, in which octahedra rotate with respect to one another,[5–8] s^2 lone-pair distortions are known to occur on the B cations of BX_6 octahedra, where B is any divalent group 14 element.[9,10] They also occur in the isoelectronic trivalent group 15 cations, such as Sb^{3+}.[11] A long-standing explanation of this effect has been to ascribe it to s- and p-orbital hybridization on the metal ions themselves, which causes the nonspherical electron distributions.[12] More recently, the importance of the anion orbitals has been recognized; it appears that the formation of a stereoactive lone pair may require their involvement.[9,10,13,14]

Of the OIPs studied here, $MAPbCl_3$ is known to possess a long-ranged, lone-pair distortion in the orientationally ordered phase stable below 172 K.[15,16] In contrast, it is known that $MAPbBr_3$ does not possess a long-ranged stereoactive lone pair in its low-temperature form.[17] None of the low-temperature structures of the phases of $MASnBr_3$ have been reported. However, the structure changes from $Pm\bar{3}m$ below 229.4 K, at which point it changes from a semiconductor to an insulator,[18] and the color changes from red to yellow; there is also spectroscopic evidence for very strong distortions of the $SnBr_3$ octahedra in the low-temperature phases of $MASnBr_3$.[19]

High-Q (where Q is the magnitude of the momentum transfer, $Q = 4\pi \sin\theta/\lambda$) X-ray powder diffraction data have been collected for atomic pair distribution function (PDF) analysis. The real-space atomic PDF, $G(r)$, gives the probability of finding pairs of atoms separated by distance r, and consists of peaks corresponding to all interatomic distances. The experimental PDF is obtained via Fourier transform (FT) of the total scattering structure function $S(Q)$, the corrected, normalized intensity from the powder scattering data, $G(r) = (2/\pi)\int_0^\infty Q[S(Q) - 1] \sin Qr \, dQ$. Unlike traditional crystallographic techniques, the PDF incorporates contributions

* Corresponding author. E-mail: Ian.Swainson@nrc.gc.ca.
[†] Michigan State University.
[‡] Canadian Neutron Beam Centre, NRC.

(1) Mitchell, R. H. *Perovskites: Modern and Ancient*; Almaz Press: Thunder Bay, ON, 2002.
(2) Mitzi, D. B. *J. Chem. Soc., Dalton Trans.* **2001**, 1.
(3) Swainson, I. P. *Acta Crystallogr., Sect. B* **2005**, *61*, 616.
(4) Mitzi, D. B.; Liang, K. *J. Solid State Chem.* **1997**, *134*, 376.
(5) Glazer, A. M. *Acta Crystallogr., Sect. B* **1972**, *28*, 3384.
(6) Glazer, A. M. *Acta Crystallogr., Sect. A* **1975**, *31*, 756.
(7) Howard, C. J.; Stokes, H. T. *Acta Crystallogr., Sect. B* **1998**, *54*, 782.
(8) Howard, C. J.; Stokes, H. T. *Acta Crystallogr., Sect. B* **2002**, *58*, 564.
(9) Seshadri, R. *Proc. Indian Acad. Sci. (Chem. Sci.)* **2001**, *113*, 487.
(10) Waghmare, U. V.; Spaldin, N. A.; Kandpal, H. C.; Seshadri, R. *Phys. Rev. B* **2003**, *67*, 125111.
(11) Zarychta, B.; Bujak, M.; Zaleski, J. *Z. Naturforsch., B* **2007**, *62*, 44.
(12) Orgel, L. E. *J. Chem. Soc.* **1959**, 3815.
(13) Payne, D. J.; Edgell, R. G.; Walsh, A.; Watson, G. W.; Guo, J.; Glans, P. A.; Learmonth, T.; Smith, K. E. *Phys. Rev. B* **2006**, *96*, 157403.
(14) Walsh, A.; Watson, G. W. *J. Phys. Chem. B* **2005**, *109*, 18868.
(15) Poglitch, A.; Weber, D. *J. Chem. Phys.* **1987**, *87*, 6373.
(16) Chi, L.; Swainson, I. P.; Cranswick, L. M. D.; Her, J.-H.; Stephens, P. W.; Knop, O. *J. Solid State Chem.* **2005**, *178*, 1376.
(17) Swainson, I. P.; Hammond, R. P.; Soullière, C.; Knop, O.; Massa, W. *J. Solid State Chem.* **2003**, *176*, 97.
(18) Onoda-Yamamuro, N.; Matsuo, T.; Suga, H. *J. Chem. Thermodyn.* **1991**, *23*, 987.
(19) Yamada, K.; Nose, S.; Umehara, T.; Okuda, T.; Ichiba, S. *Bull. Chem. Soc. Jpn.* **1988**, *61*, 4265.

10.1021/cm702668d CCC: $40.75
Published on Web 01/24/2008

from both Bragg and diffuse scattering intensities contained in $S(Q)$, providing local structural information.[20,21]

In this paper we report the results of a PDF study examining differences in local structure as a function of composition across a set of perovskites, all of which are in the $Pm\bar{3}m$ phase. The A cations are known to be dynamically disordered in this phase and therefore do not form static hydrogen bonds with the halides.[22] We were especially interested in evidence of localized distortions of the BX_6 octahedra in the $Pm\bar{3}m$ phase and in comparing this to what is known about long-ranged distortions in the low-temperature phases.

Experimental Method

X-ray powder diffraction data for PDF analysis were collected at the 6IDD MUCAT beamline at the Advanced Photon Source (APS) at Argonne National Laboratory in the rapid acquisition PDF mode (RAPDF).[23] Five samples of perovskites with A sites containing methylammonium (MA), $CH_3NH_3^+$, and formamidinium (FA), $NH_2{-}CH{=}NH_2^+$, and where X = Cl or Br and B = Pb^{2+} or Sn^{2+}, were measured: $MAPbBr_3$, $MAPbCl_3$, $MASnBr_3$, $FAPbBr_3$, and $FA_{0.5}MA_{0.5}PbBr_3$. X-ray PDFs were chosen in place of neutron PDFs, since the former are dominated by scattering from the heavy inorganic components. The triplet of partial pairs B−B, B−X, and X−X generate 77–82% of total scattering, depending on the composition. The remaining scattering is distributed across 12 partial pair distributions: (i) Intramolecular distances within the rigid A cations. The six partials between C, N, and H are expected to be sharp, but sum to <1.6% of total scattering, are confined to r < 1.55 Å, and can therefore be ignored. (ii) Distances between atoms in the A cations and the B and X atoms. No partial pair distribution between component atoms of A and either B or X exceeds 6.5% of total scattering. Since the A cations rotate dynamically at room temperature,[22] these partial pair distributions are not sharp. Therefore, the only sharp correlations with any significant weighting come from the inorganic component.

Each sample was ground and packed to a thickness of 1.0 mm in a circular stainless steel holder of diameter 5 mm and sealed with kapton tape. X-ray data were collected at room temperature using a 86.727 keV (λ = 0.142 96 Å) beam. A Mar345 image plate camera with diameter of 345 mm was mounted orthogonal to the beam with sample–detector distance of 210.44 mm. Depending on the sample the image plate was repeatedly exposed for between 4 and 10 s for 4−7 times, to improve the counting statistics. The patterns were inspected for impurities and to check that the compound was in the $Pm\bar{3}m$ phase. A representative image is shown in Figure 1. The two-dimensional data sets were integrated and converted to intensity vs 2θ format, $I(2\theta)$, using the program Fit2D,[24] where 2θ is the angle between the incident and scattered X-rays. The $I(2\theta)$ data were normalized by the average monitor counts. Using the PDFgetX2 software package,[25] data from an empty container were subtracted from the raw data, and various other corrections were applied as described in detail in ref 21. The total scattering function $S(Q)$ was obtained and truncated at a maximum momentum transfer of Q_{max} = 20.0 Å^{-1}. The Q_{max} of 20.0 Å^{-1} was selected because beyond $Q \approx$ 20.0 Å^{-1}, the signal-to-noise ratio was unfavorable. The PDF, $G(r)$, was then derived by Fourier transform of the $S(Q)$. All the $S(Q)$ and PDFs were of good quality and are shown in Figure 2.

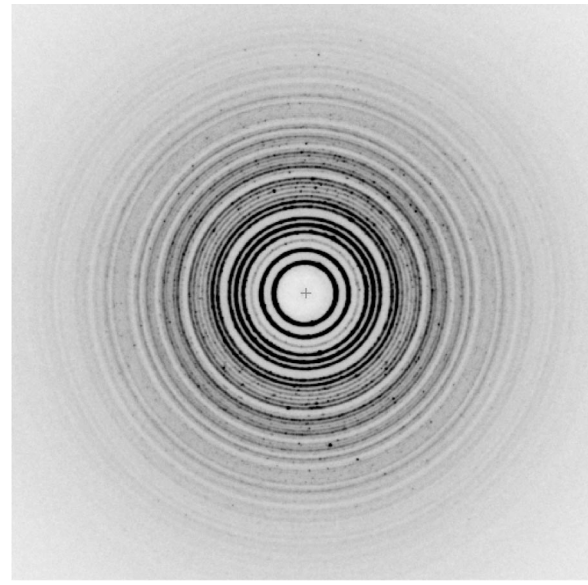

Figure 1. Representative Mar345 image obtained from $MAPbCl_3$. Note the well-defined Debye−Sherrer rings, indicating good data quality. A check was made for each of the materials that no extra lines were present that were not explicable on the basis of the $Pm\bar{3}m$ cell.

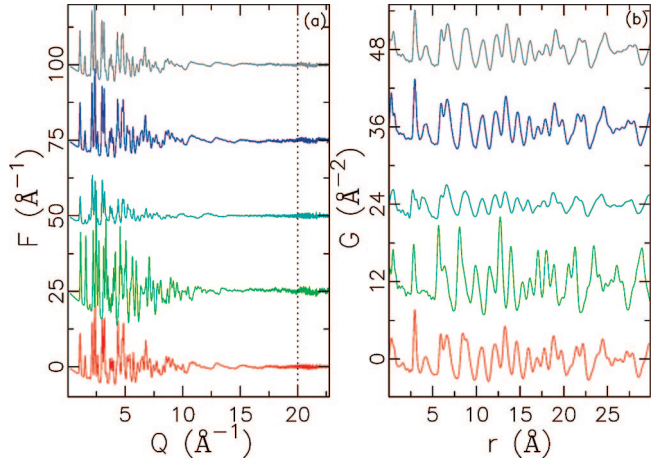

Figure 2. (a) Experimental reduced structure function $F(Q) = Q(S(Q) - 1)$ of all samples and (b) the corresponding PDFs, using a Q_{max} of 20.0 Å^{-1} (dotted line).

The refinement program PDFFit2[26] was used to analyze the local distortions present in the structure, using least-squares refinement methods in the range from 2 to 19 Å. Modeling the A cation was approximated by placing a pseudoatom of appropriate scattering power at the geometric center of the cation and giving it a large Debye–Waller factor. Two sets of models were refined for each sample. The first models were based on a single $Pm\bar{3}m$ unit cell, while the second models were formed from a 2 × 2 × 2 supercell of the primitive cubic lattice. Two sets of bond angles were

(20) Billinge, S. J. L.; Kanatzidis, M. G. *Chem. Commun.* **2004**, 749.
(21) Egami, T.; Billinge, S. J. L. *Underneath the Bragg Peaks: Structural Analysis of Complex Materials*; Pergamon Press: Oxford, England, 2003.
(22) Knop, O.; Wasylishen, R. E.; White, M. A.; Cameron, T. S.; Van Oort, M. J. M. *Can. J. Chem.* **1990**, *68*, 412.
(23) Chupas, P. J.; Qiu, X.; Hanson, J. C.; Lee, P. L.; Grey, C. P.; Billinge, S. J. L. *J. Appl. Crystallogr.* **2003**, *36*, 1342.
(24) Hammersley, A. P.; Svenson, S. O; Hanand, M.; Hauserman, D. *High Pressure Res.* **1996**, *14*, 235.
(25) Qiu, X.; Thompson, J. W.; Billinge, S. J. L. *J. Appl. Crystallogr.* **2004**, *37*, 678.
(26) Farrow, C. L; uhas, P.; Liu, J. W.; Bryndin, D.; Bozin, E. S.; Bloch, J.; Proffen, Th.; Billinge, S. J. L. *J. Phys.: Condens. Matter* **2007**, *19*, 335219.

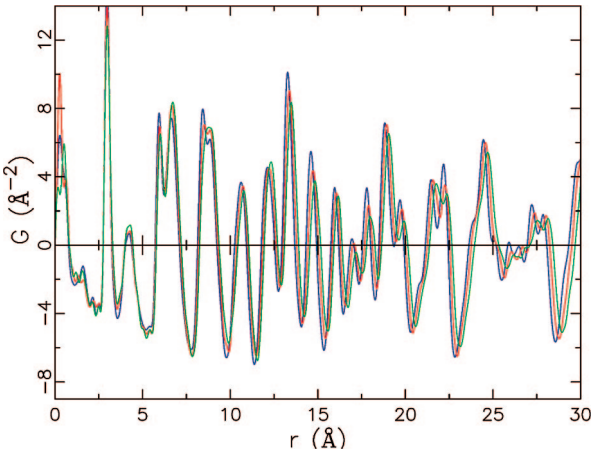

Figure 3. Comparison of the variation of experimental PDFs as a function of varying the organic cation: $MAPbBr_3$ (blue), $FA_{0.5}MA_{0.5}PbBr_3$ (red), and $FAPbBr_3$ (green).

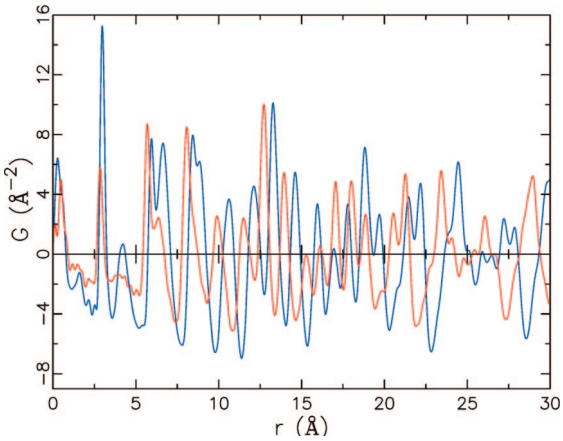

Figure 4. Comparison of experimental PDFs obtained from samples with different halides. $MAPbBr_3$ (blue) and $MAPbCl_3$ (red).

extracted from each refinement: intraoctahedral X−B−X bond angles, a measure of internal distortion of the octahedra, and interoctahedral B−X−B angles, which include contributions from external conformations of the octahedra, such as tilts. The idealized crystallographic model of perovskite requires B and X atoms constrained to special equivalent positions, allowing no tilting, distortion of octahedra, or stereoactive lone pair on B, so that the B−X−B angles are 180°.

Results and Discussion

Qualitative Observations. We first discuss qualitative observations of the PDFs of the Pb-containing materials. The first peak in the PDF at $r = 2.8$ Å (Figure 3) is the Pb−X distance, and it is quite sharp. The second peak represents the shortest X−X distances along the edges of the PbX_6 octahedra and is broad in all the materials, suggesting that the BX_6 octahedra are not very rigid in general. The peak near 6 Å is from Pb−Pb correlations across neighboring octahedra. This peak is also sharp, suggesting that the center−center distance between neighboring octahedra is a well-defined quantity, despite the disorder on the halide site. The broad X−X, sharp Pb−X, and Pb−Pb distributions can be reconciled if there is strong internal angular deformation of the octahedra; i.e., the X−Pb−X angle changes from the ideal 90°.

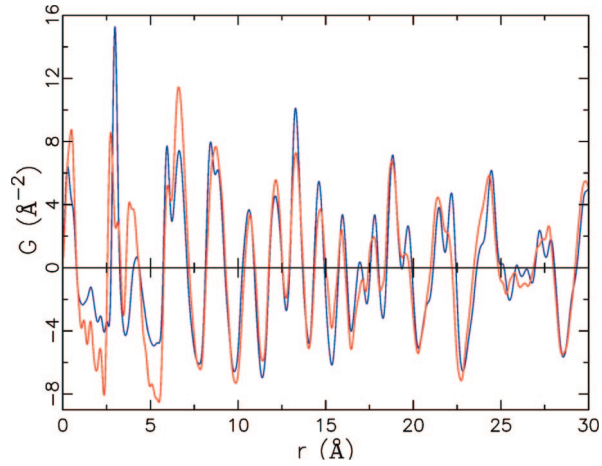

Figure 5. Comparison of the variation of PDFs obtained from samples with different B-site composition: $MAPbBr_3$ (blue) and $MASnBr_3$ (red), scaled for comparison.

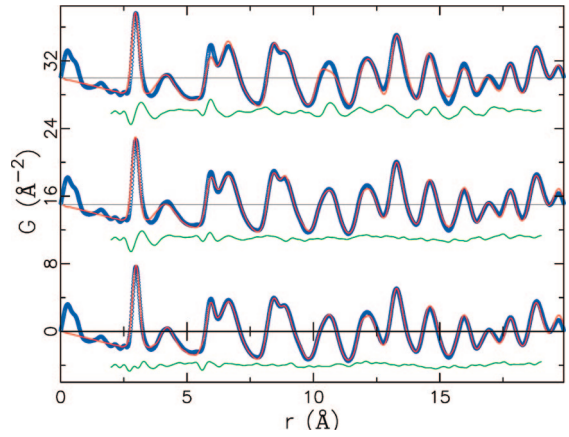

Figure 6. Calculated PDF from the refined single cell model of $MAPbBr_3$, using (top) isotropic ADPs and (middle) anisotropic ADPs. The PDFs of the models (red), the PDF data (blue), and a difference plot (green) is shown underneath across the region refined, i.e., 2–19 Å. The PDF for the final single cell model of the same sample is shown on the bottom, with no offset.

Table 1. Atomic Displacement Parameters, Lattice Constant, and Fit Strength of the Single Cell Structure Models Obtained from Samples with MA Cations[a]

	$MAPbBr_3$	$MAPbCl_3$	$MASnBr_3$
a, Å	5.9311224(4)	5.685168(3)	5.907687(8)
B U_{iso}, 10^{-2} Å^2	2.5646(3)	2.3625(2)	5.248(3)
X $U_{\|\|}$, 10^{-2} Å^2	0.4597(9)	0.0047(4)	1.577(1)
X $U_{\perp}$, 10^{-2} Å^2	7.008(2)	7.230(5)	8.726(4)
A U_{iso}, 10^{-2} Å^2	15.86(2)	14.97(1)	47.86(7)
R_w, %	9.58	11.50	29.05

[a] X $U_{||}$ refers to the anisotropic ADPs of each halide along B−X direction, and X $U_{\perp}$ refers to the component perpendicular to that same direction. a refers to the cubic lattice parameter.

The effect of changing the A cation in the $APbBr_3$ (A = MA, FA) solid solution has little effect on the local structure (Figure 3). Any differences in the widths of the Pb−Pb and X−X peaks are imperceptible; only a rather small change in lattice parameter is evident by small relative shifts of the PDFs at high r. The AX_{12} cage sizes are therefore very similar and evidently of sufficient volume that both MA and FA can undergo nearly free rotation. This gives us confidence that the changes we see across the PDFs of other OIPs are significant.

Table 2. Atomic Displacement Parameters, Lattice Constant, and Fit Strength of the Final Refined Structure Models Obtained from Each of the Samples[a]

	$MAPbBr_3$	$MAPbCl_3$	$FA_{0.5}MA_{0.5}PbBr_3$	$FAPbBr_3$	$MASnBr_3$
a, Å	11.853948(6)	11.351040(5)	11.913707(9)	11.988867(6)	11.83309(2)
B U_{iso}, 10^{-2} Å^2	2.4529(2)	2.1147(2)	3.0003(3)	3.6651(3)	4.5527(8)
X $U_{\|\|}$, 10^{-2} Å^2	0.4201(3)	0.1795(7)	0.3728(3)	0.8123(7)	0.6920(7)
X $U_{\perp}$, 10^{-2} Å^2	3.8446(7)	0.8751(8)	3.1297(9)	1.9451(7)	4.959(2)
A U_{iso}, 10^{-2} Å^2	4.256(6)	16.218(6)	8.626(7)	13.884(6)	3.360(7)
R_w, %	8.36	9.71	8.02	9.76	10.77

[a] X $U_{||}$ refers to the anisotropic ADPs of each halide along the B−X direction, and X $U_{\perp}$ refers to the component perpendicular to that same direction. *a* refers to the lattice constant of the 2 × 2 × 2 supercell.

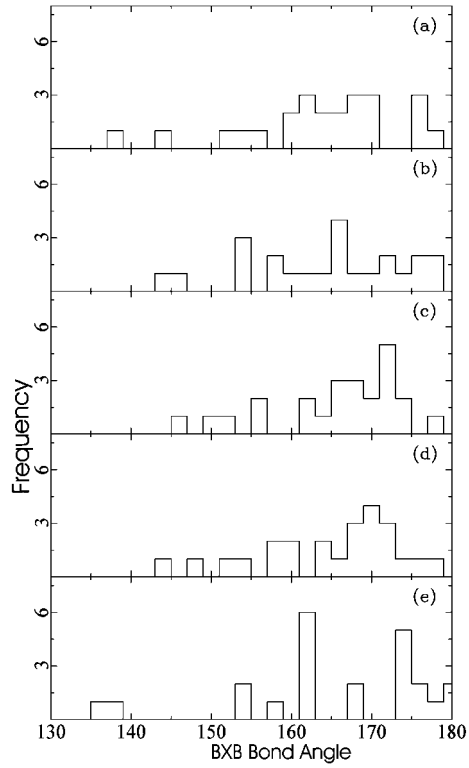

Figure 7. Histograms of the distributions of B−X−B bond angles between octahedra in the final refined models of (a) $MAPbBr_3$, (b) $MAPbCl_3$, (c) $FA_{0.5}MA_{0.5}PbBr_3$, (d) $FAPbBr_3$, and (e) $MASnBr_3$.

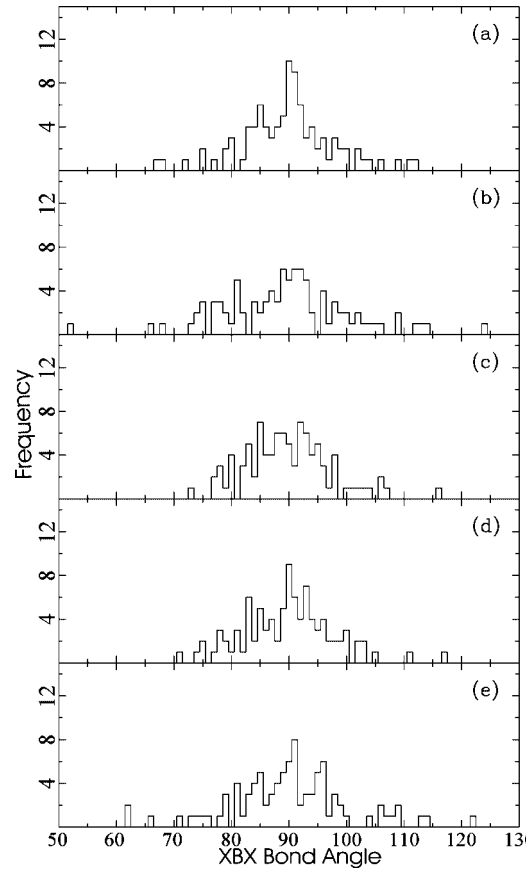

Figure 8. Histograms of the distributions of X−B−X bond angles of each octahedron in the final refined models of (a) $MAPbBr_3$, (b) $MAPbCl_3$, (c) $FA_{0.5}MA_{0.5}PbBr_3$, (d) $FAPbBr_3$, and (e) $MASnBr_3$.

Changing the halide in $MAPbX_3$ (X = Br, Cl) inevitably produces a large change in lattice parameter, with the chloride having the smallest cell (Figure 4). The X−X distribution around $r = 4$ Å is weaker, since its weighting is lower, but it is also much broader in the chloride than in any $APbBr_3$. However, the Pb−Pb correlations remain sharp, suggesting strong internal deformation of the octahedra but a well-defined unit cell. The Pb−X distribution is distinctly asymmetric for the chloride compared to all $APbBr_3$.

Changing the B site in the pair $MABBr_3$ (B = Pb, Sn) has a small effect on the PDF and the structure, as shown in Figure 5. The B−B correlations near 6 Å produce a much smaller peak in the PDF of $MASnBr_3$ than in that of $MAPbBr_3$, as Sn has a much smaller atomic number. However, the various correlations contributing to the nearby peaks at 8.4 and 8.8 Å in $MAPbBr_3$ broaden into a single peak in $MASnBr_3$, suggesting that $MASnBr_3$ may be more disordered.

Single Unit Cell Refinement. Fits using isotropic atomic displacement parameters (ADPs) were universally poor. For example, the weighted agreement factor[26] for the fit to $MAPbBr_3$ with isotropic ADPs was $R_w = 20.0\%$ (Figure 6, top). The model was modified to refine separate components of ADPs for the halide atoms, transverse and parallel to the B−X bond. The values of the ADPs parallel to the B−X bond axis were much smaller than those perpendicular to it. Using these modifications alone, the agreement factors are significantly reduced ($R_w = 13.8\%$) and a better quality of fit is obtained (Figure 6, middle). These anisotropic ADPs show that the halides are transversely displaced off their ideal positions that lie midway along the B−B line. It is likely that the local position of the halide has only a very small probability of coinciding with the ideal crystallographic position, as in the high-symmetry framework of tetrahedra of β-cristobalite.[27] We therefore allowed the halides to move off the special equivalent position, which further improved the fit and reduced the size of the transverse component of

(27) Swainson, I. P.; Dove, M. T. *Phys. Rev. Lett.* **1993**, *71*, 193.

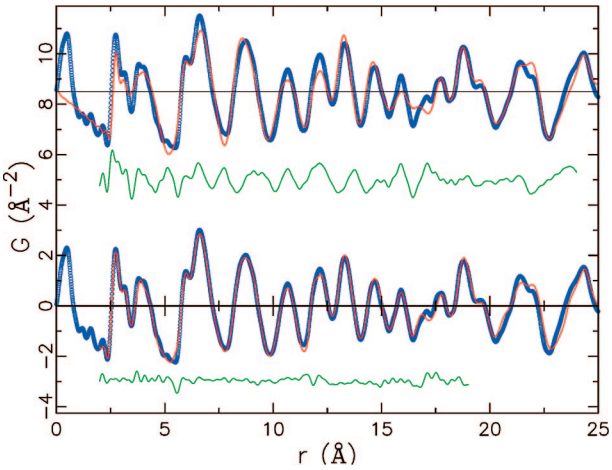

Figure 9. Resulting PDFs of the models of $MASnBr_3$ using (upper) a single unit cell model and (lower) a 2 × 2 × 2 supercell model. The experimental PDF (blue), the refined models (red), and a difference plot (green) is shown underneath the area refined. The single cell model was refined from 2 to 24 Å rather than the 2–19 Å range used for all other refinements. This was necessary to stabilize the refinement of the lattice constant *a*.

their ADPs. The halide ADPs in these single cell models were for the most part extremely anisotropic; e.g., in $MAPbCl_3$ the ADPs of chlorides were found to be 0.072 30 Å^2 perpendicular to the Pb−Cl axes and 0.000 047 Å^2 parallel to them (Table 1).

In $MAPbCl_3$ the Pb−Cl distribution is distinctly asymmetric. It was necessary to allow the lead atom to be displaced from the center of the octahedron in order to achieve a reasonable fit; the final displacement was 0.27 Å. None of the other samples showed significant improvement when the B was allowed to move off-center, with the notable exception of $MASnBr_3$. The Sn−Br distribution appears bifurcated (Figure 5), something not seen in any of the other PDFs. There is a distinct possibility that tin is off-center in this case.

No fit to any PDF showed improvement when the model was allowed to become metrically noncubic. In all samples it was found that the ADPs of the A-site pseudoatom could be reduced if its position was refined, although the weak scattering and crude approximation to the shape of the molecular cation makes it difficult to conclude with certainty that this is significant. The refinement of $MASnBr_3$ did not yield favorable results even when the Br positions were permitted to refine in all three dimensions, and no single cell model of $MASnBr_3$ produced a satisfactory fit to the PDF.

Large ADPs in a refinement often indicate that atomic positions have not been perfectly determined, either due to not being refined or to the real structure being distorted in a way not describable with the symmetry used by the model.

2 × 2 × 2 Supercell Refinements. A single cell can represent only ferrodistortive local order, and antiferrodistortive local order, such as tilting, cannot be described this way. Therefore, we extended the modeling to incorporate antiferrodistortions in a 2 × 2 × 2 supercell. After giving the positions of the halide atoms a slight random displacement, the positions of the halides and then the A pseudoatom were refined, followed by refining the halide positions once more. The results are summarized in Table 2. An attempt was made to refine the positions of the B atoms in the supercell, but this had only a significant effect in the case of $MAPbCl_3$.

The distributions of B−X−B and X−B−X bond angles from the supercell refinements are shown in Figure 7 and Figure 8, respectively. All the final refinements found substantial distortion, shown by the rather large spread of bond angles away from 180° for the B−X−B angles and from 90° for the X−B−X angles. While the sampling of such a distribution is sparse, the $MASnBr_3$ and $MAPbCl_3$ samples appear to have the largest spread. Off-center displacement of the Pb in $MAPbCl_3$ causes additional distortion of the X−B−X angles compared to those seen in $MAPbBr_3$. $MASnBr_3$ yielded a particularly unusual, roughly bimodal distribution of B−X−B angles. The description of the $MASnBr_3$ PDF was significantly improved in the supercell compared to the single cell description, and the component of Br ADPs transverse to the Sn−Br axes was strongly reduced (Table 2, Figure 9).

The benefit of the extra parameters to describe more complex local distortions also makes the refinements underconstrained, and it is possible that models with the minimum R_w do not correspond to realistic structure models. This, and our exclusion of rigorously modeling the organic component, represents the main limitation to how quantitative our modeling can become.

Conclusions

The local structures of a series of selected OIPs showed strong, generally angular, internal distortions of octahedra. This showed that the local environment of the octahedron is far from the undeformed model inferred from a traditional crystallographic description of the $Pm\bar{3}m$ structure, in which they all crystallize. Refinements showed that the halides had a significant displacement transverse to the midpoint of the B−B line (to which they are constrained in the ideal crystallographic description). These displacements are likely dynamic in nature due in part to the presence of soft transverse acoustic phonons in these structures.[3,28]

Changing the halide in $MAPbX_3$ (X = Br, Cl) had a significant impact on the local structure. The volume of the chloride cell is significantly smaller and is the only Pb compound in which there is an asymmetric Pb−X distribution. Models could only explain this by displacing Pb^{2+} from the center of the octahedron. This is the first structural evidence of local lone pair distortions in an OIP in the $Pm\bar{3}m$ phase. A bifurcated Sn−Br distribution is also seen, suggesting similar distortions may exist in $MASnBr_3$, but the refined supercell model for $MASnBr_3$ had an unusual distribution of bond angles. This may suggest that the disorder in $MASnBr_3$ is more complex than can be described even in the 2 × 2 × 2 supercell.

(28) Giddy, A. P.; Dove, M. T.; Pawley, G. S.; Heine, V. *Acta Crystallogr., Sect. A* **1993**, *49*, 697.

Acknowledgment. We acknowledge Ahmad Masadeh, Pavol Juhas, Emil Bozin, Gianluca Paglia, Asel Sarbaeva, Mouath Shatnawi, He Lin, and Moneeb Shatnawi for help in collecting data. This work was supported in part by National Science Foundation (NSF) grant DMR-0304391. Data were collected at the 6IDD beamline in the Midwest Universities Collaborative Access Team (MUCAT) sector at the Advanced Photon Source (APS). Use of the APS is supported by the U.S. DOE, Office of Science, Office of Basic Energy Sciences, under Contract W-31109-Eng-38. The MUCAT sector at the APS is supported by the U.S. DOE, Office of Science, Office of Basic Energy Sciences, through the Ames Laboratory under Contract W-7405-Eng-82.

CM702668D